

Raman scattering by pure water and seawater

Jasmine S. Bartlett, Kenneth J. Voss, Shubha Sathyendranath, and Anthony Vodacek

Measurements of the magnitude and spectral distribution of the Raman-scattering coefficients of pure water (b_{rw}) and seawater (b_{rs}) are presented. Two independent measurements of the spectral distribution of the Raman-scattering coefficient of pure water were made for incident wavelengths ranging from 250 to 500 nm. These measurements revealed a strong dependence of b_{rw} on wavelength that could be represented by a $(\lambda')^{-5.3 \pm 0.3}$ relationship, where λ' is the incident wavelength, or a $\lambda^{-4.6 \pm 0.3}$ relationship, where λ is the Raman-scattered wavelength, when normalized to units of photons. The corresponding relationships for normalization to energy are $(\lambda')^{-5.5 \pm 0.4}$ and $\lambda^{-4.8 \pm 0.3}$, respectively. These relationships are found to be consistent with resonance Raman theory for an absorption wavelength of 130 nm. The absolute value of b_{rw} for the 3400-cm⁻¹ line was found to be $(2.7 \pm 0.2) \times 10^{-4}$ m⁻¹ for an incident wavelength of 488 nm, which is consistent with a number of earlier reports. The difference between the magnitudes of the Raman-scattering coefficients for pure water and seawater was statistically insignificant. © 1998 Optical Society of America

OCIS codes: 190.5650, 290.0290, 290.5860, 290.5820, 010.7340, 010.4450.

1. Introduction

Many applications in the field of oceanography, such as the estimation of primary production¹ and new production,² and the determination of heat budgets for the oceanic mixed layer,³ require estimates of pigment biomass at large spatial scales. Pigment biomass is generally estimated from satellite-based determinations of ocean color. However, factors other than pigment biomass are known to influence sea surface reflectance, whose spectral variations determine ocean color. One of these factors is Raman scattering by seawater. Interpretations of ocean-color data can be improved by accounting for the contribution of Raman scattering by seawater to reflectance. Similarly, the spectral characteristics of the underwater light field can be assessed more accurately by incorporating the effects of Raman scattering by seawater. To address these points, a number of models incorporating Raman scattering

have been derived.⁴⁻¹⁰ Discussions of these models can also be found in Mobley¹¹ and Bartlett.¹²

Recently it has been shown that Raman scattering by seawater may have a substantial effect on measurements of sea surface reflectance for wavelengths (λ) in the visible wavelength region.^{4,5,9,13-20} It may be responsible for as much as 30% of the sea surface reflectance measured in the 500-700-nm wavelength region.^{5,18-20} Raman scattering is an inelastic-scattering process; when the scattering medium is water, it occurs with approximately one tenth of the probability of an occurrence of elastic scattering by water. The Raman-scattering process can be described as follows: A photon with a given energy is incident on the scattering molecule, which immediately scatters a photon with an energy different from that of the incident photon. The difference in energy between the incident and scattered photons, which can be either positive or negative, corresponds to that between two energy levels of the molecule. For a given pair of energy levels, the energy difference can be expressed in terms of either a constant frequency difference (such as 3400 cm⁻¹ for the OH stretch vibrational mode²¹ in water) or a variable wavelength difference between the incident and scattered photons. To quantify the potential effect of Raman scattering by seawater on remote measurements of ocean color, it is necessary to know its magnitude and its spectral variability.

Attempts to quantify the effect of Raman scattering on ocean color have been hampered by a lack of agreement between investigators on the absolute magni-

J. S. Bartlett is with the College of Oceanic and Atmospheric Sciences, Oregon State University, Corvallis, Oregon 97331. K. J. Voss is with the Department of Physics, University of Miami, Coral Gables, Florida 33124. S. Sathyendranath is with the Bedford Institute of Oceanography, P.O. Box 1006, Dartmouth, Nova Scotia B2Y 4A2, Canada. A. Vodacek is with the Department of Chemistry and Biochemistry, University of Maryland, College Park, Maryland 20742.

Received 4 June 1997; revised manuscript received 12 January 1998.

0003-6935/98/153324-09\$15.00/0

© 1998 Optical Society of America

tude and wavelength dependence of the Raman-scattering coefficient for seawater [$b_{rs}(\lambda)$]. In previous studies, $b_{rs}(\lambda)$ has been approximated by $b_{rw}(\lambda)$, the Raman scattering coefficient for pure water, and it has been suggested that these coefficients may differ from each other by as much as 10%.⁴ The magnitude of $b_{rw}(\lambda)$ itself is in dispute: Experimental estimates of the Raman-scattering cross section for pure water at 90° for an incident wavelength of 488 nm, which is proportional to $b_{rw}(488)$, differ by a factor of 5.^{5,13,21–27} Furthermore, the spectral characteristics of $b_{rw}(\lambda)$ are poorly known^{11,25–27}: both λ^{-4} and λ^{-5} dependencies have been used for both the incident and the scattered wavelengths.^{6–9,13,19} We report new data on the spectral variability and magnitude of the Raman-scattering coefficients for pure water and seawater.

2. Wavelength Dependence of the Raman-Scattering Coefficient for Pure Water

In this paper we present two independent sets of measurements of the wavelength dependence of the Raman-scattering coefficient for pure water using two instruments. The first results presented here were determined with a Quantamaster luminescence spectrometer, Model QM-1, from Photon Technology International, Inc. (PTI), London, Ontario, Canada. The second results were determined with an Hitachi spectrofluorometer. The general experimental setup is described first. Details of the calibration procedures used for each of the instruments is then presented, followed by the results from each experiment.

A. General Experimental Setup and Calibration

Both instruments used in this study were configured to measure Raman-scattering spectra at 90° to a beam of finite bandwidth incident on a sample. Light from the source (a xenon lamp) is passed through a grating monochromator to select the incident wavelength. The samples are held in quartz cuvettes with 1-cm path lengths. Variable slits in the light path before and after the sample are used to alter the bandpass. Glan-Thompson polarizers are used to polarize the incident beams and scattered beams perpendicular to the scattering plane. The scattered light from the sample then passes through another grating monochromator that measures the emission spectrum over a selected wavelength region. The intensity of the scattered light is monitored by a photomultiplier. This configuration is similar to that of Marshall¹⁶ and Marshall and Smith.⁵ Both experiments used triply distilled water at room temperature (20 °C).

Raman emission spectra for different incident wavelengths cannot be compared unless each of these spectra has been normalized to the same excitation intensity. Fluctuations in the intensity of the source irradiance are monitored by use of a beam splitter to direct a portion of the incident light to a reference photomultiplier. We determined the spectral characteristics of this photomultiplier and of the beam

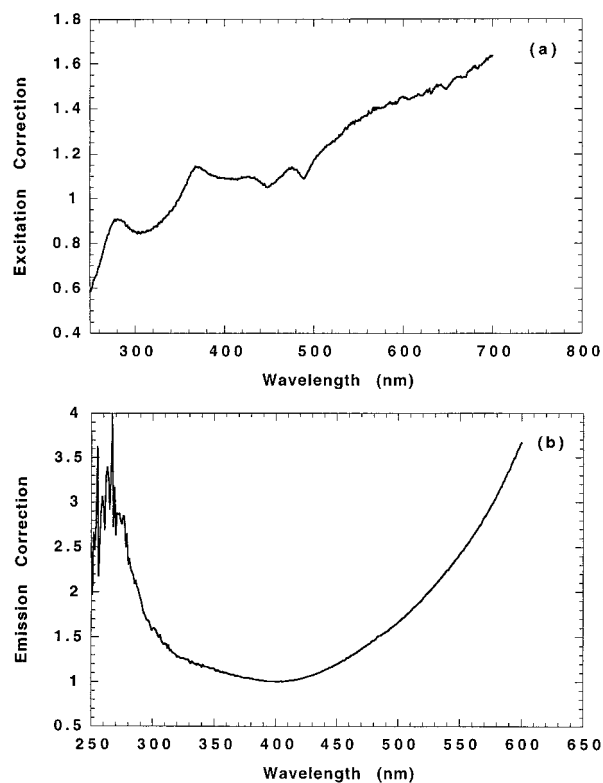


Fig. 1. Correction curves for the PTI spectrofluorometer with the polarizers in place for (a) the excitation optics and (b) the emission optics.

splitter by performing calibrations with Rhodamine B, which is a strong absorber with a quantum yield that is approximately constant in the 200–600-nm region. The calibration procedure for the excitation spectrum was as follows: A right-angle, triangular quartz cuvette containing Rhodamine B (8 g/L in propylene glycol) was placed in the sample holder with the largest face oriented toward the incident light in such a way that the light reflected off this face of the cuvette was directed away from the emission monochromator. An excitation scan from 250 to 700 nm was then made for an emission wavelength of 630 nm (the wavelength of maximum fluorescence of Rhodamine B) with the excitation polarizer in place. The ratio of the signal recorded by the reference photomultiplier [$I_{\text{ref}}(\lambda')$] to that recorded by the emission photomultiplier [$I_{\text{rhod}}(\lambda')$] for the same incident wavelengths provides an excitation correction curve [$C_{\text{ex}}(\lambda')$] that accounts for the spectral characteristics of the reference photomultiplier and of the optical components between the reference photomultiplier and the sample:

$$C_{\text{ex}}(\lambda') = I_{\text{ref}}(\lambda')/I_{\text{rhod}}(\lambda'). \quad (1)$$

An example of an excitation-correction curve for the PTI instrument is shown in Fig. 1(a). Each measured emission spectrum was scaled by the value of the excitation correction factor for the incident wavelength.

We found a correction curve for the spectral re-

sponse of the instrumental components in the emission monochromator in the PTI instrument by calibrating the instrument with a standard tungsten lamp. The calibration procedure was as follows: The standard tungsten lamp was positioned such that the emitted light was incident normal to the sample holder and at 90° to the emission light path. There were no optical components between the lamp and the sample. An empty, frosted quartz cuvette, with a 1-cm path length, was placed in the sample holder. An emission spectrum was then measured with the emission polarizer in place. To determine the contribution from stray light, a dark measurement was also made with the lamp turned off. This dark measurement was then subtracted from the lamp measurement. The resulting emission spectrum is measured in units of photon counts per second (cps), whereas the units of the standard lamp spectrum is in terms of energy. From the relationship $E = hc/\lambda$, where E is the photon energy, h is Planck's constant, and c is the speed of light, energy can be converted to photon counts by dividing by hc/λ . Because only a relative calibration is required for this experiment, we achieved the conversion of the standard lamp spectrum from energy units to cps by multiplying by λ . The ratio of the standard spectrum of the lamp in units of cps [$I_{\text{lamp}}(\lambda)$] to the dark-corrected emission spectrum [$I_{\text{em}}(\lambda)$] yields an emission correction curve [$C_{\text{em}}(\lambda)$] that accounts for the spectral characteristics of optical components in the path of the emitted light:

$$C_{\text{em}}(\lambda) = I_{\text{lamp}}(\lambda)/I_{\text{em}}(\lambda). \quad (2)$$

Figure 1(b) shows an example of an emission correction curve for the PTI instrument in this configuration. The low irradiances of the standard lamp in the 250–300-nm region, particularly with the polarizer in place, caused the signal in this region to be noisy and sensitive to small changes in the background correction, making it difficult to obtain an accurate calibration in this region [Fig. 1(b)]. All the Raman emission spectra presented here were corrected for spectral variations in the emission response of the spectrometer by multiplying each measured emission spectrum by the emission correction spectrum. Data from the 250–300-nm region were retained here for completeness, although we recognize that these results are less reliable than those from longer wavelengths.

We calibrated the Hitachi emission optics by performing a synchronized scan with the excitation and emission monochromators of a neutral glass diffuser. Dark values were first subtracted from this data, and then the excitation corrections were performed. The resulting signal is the wavelength dependence of the emission optics. This signal was used to form an emission correction factor for this instrument.

We thus obtained corrected emission spectra [$I_{\text{corr}}(\lambda', \lambda)$] by multiplying each measured emission spectrum [$I_{\text{meas}}(\lambda', \lambda)$] by the value of the excitation

correction at the incident wavelength and by the emission correction spectrum:

$$I_{\text{corr}}(\lambda', \lambda) = I_{\text{meas}}(\lambda', \lambda)C_{\text{ex}}(\lambda')C_{\text{em}}(\lambda). \quad (3)$$

The quantity $I_{\text{meas}}(\lambda', \lambda)$ represents a raw emission spectrum normalized to a reference to account for fluctuations in the intensity of the incident light. Because both the raw emission spectrum and the reference are measured in units of photon counts, $I_{\text{meas}}(\lambda', \lambda)$ is normalized to these units. To obtain a corrected spectrum normalized to energy units, the raw emission spectrum and the reference values must be converted to energy units. This can be achieved by multiplying $I_{\text{meas}}(\lambda', \lambda)$, and hence $I_{\text{corr}}(\lambda', \lambda)$, by λ'/λ . Because the relationship between λ' and λ can be approximated by $\lambda = 0.53(\lambda')^{1.13}$ in the wavelength region studied here,²⁰ the ratio λ'/λ is approximately equal to $1.75(\lambda)^{-0.12}$ or $1.89(\lambda')^{-0.13}$. The corrected spectrum used must be appropriate to the units of the study. For example, Monte Carlo simulations of the Raman-scattering process should use the results presented here in units of photon counts, whereas radiative transfer applications should use those in energy units. An analysis of the calibration procedures described here can be found in Hofstraat and Latuhihin.²⁸

B. Experimental Details and Results

1. Photon Technology International Spectrofluorometer

Raman scattering at 90° with a bandpass of 5 nm was measured for several samples of triply distilled water for incident wavelengths covering the 250–500-nm range. This corresponds to Raman peaks in the 260–600-nm range for the 3400-cm⁻¹ Raman band for water. The results for one of these pure water samples are shown in Fig. 2(a). The increase in background light for wavelengths shorter than 300 nm is caused by the proximity of the Rayleigh peak to the Raman peak at these wavelengths.

To determine the relationship between the total intensity of the Raman-scattered signal normalized to units of energy and λ' , the Raman peak for each incident wavelength was integrated to obtain the peak area, and the results were then plotted as a function of λ' [Fig. 2(b)]. This figure shows the results from six repetitions of the experiment. These results are integrated values for incident light with a bandpass of 5 nm. However, in the wavelength region studied, the difference between these results and an explicit integration over the incident wavelength is negligible,²⁹ hence the results presented here are applicable to most spectral applications. One exception, however, may be narrow-band applications such as those involving laser excitation.

According to theory,^{30,31} the intensity (in units of watts) of Raman scattering by all substances should follow a λ^{-4} law in the wavelength region studied here, except near an absorption band. Fitting a power function in λ' to the $b_{rw}(\lambda')$ data normalized to

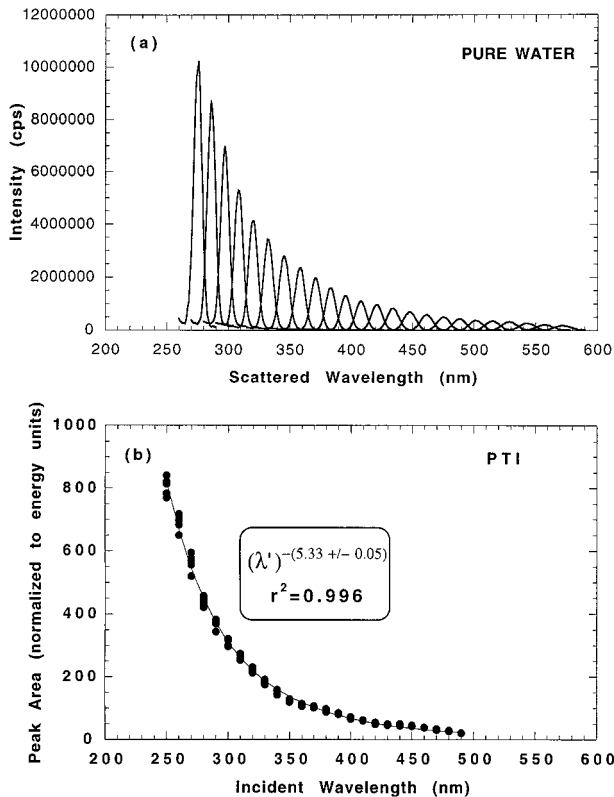


Fig. 2. (a) Spectra resulting from Raman scattering by pure water for incident wavelengths ranging from 250 to 500 nm at a bandpass of 5 nm. These measurements were made with a PTI spectrofluorometer. (b) Relationship between the peak areas, normalized to energy units, for Raman scattering by pure water at a 5-nm bandpass and the incident wavelength for six water samples (solid circles). The data are best fit by a $(\lambda')^{-5.33}$ power law (solid curve, $r^2 = 0.996$).

energy units shown in Fig. 2(b) gave an excellent fit ($r^2 = 0.996$), with an exponent of -5.33 ± 0.05 . The difficulties that were encountered with measurements for incident wavelengths in the 250–300-nm region made the results in this spectral region less reliable than at longer wavelengths. These difficulties were twofold: First, as described above, there were problems with establishing the emission correction spectrum for this region [Fig. 1(b)]; second, the proximity of the Rayleigh peaks to the corresponding Raman peaks is a potential source of error in the peak-area calculations for this part of the spectrum. However, when the curve fitting was repeated excluding the data from this region, the fitted exponent did not change. To express the results as a function of λ ,

the Raman-scattered wavelength, we repeated the curve fitting using $b_{rw}(\lambda)$ and λ , which yielded a wavelength dependence of $\lambda^{-(4.80 \pm 0.04)}$ with an r^2 of 0.996 (Table 1). The value of this fitted exponent is closer to the experimental value of -5 that has been reported based on measurements for incident wavelengths in the 400–550-nm region by Sugihara *et al.*¹³ than the value of -4 expected from theoretical considerations.^{30,31}

2. Hitachi Spectrofluorometer

Three separate data-collection series were run, and instrument calibrations were performed before each data series. In addition, data were collected after each measurement, mimicking the measurement conditions in which the receiver optics was blocked. This allowed an accurate dark series to be obtained, which was subtracted from the measurements.

Raman spectra were obtained by selecting an incident wavelength and scanning the region of the Raman-scattered spectrum. This was repeated for several incident wavelengths from 275 to 475 nm (every 25 nm). Often the Raman signal would lie on top of another more slowly decaying signal. Portions of the signal on either side of the Raman band were selected to provide a baseline, and this baseline was subtracted from the data. The remaining signal was then integrated to find the relative magnitude of the total Raman signal. Each data run was normalized to the result obtained with an incident wavelength of 475 nm and a power fit was then made to the data (Fig. 3). The resulting exponent values are summarized in Table 1.

C. Comparison of Two Independent Sets of Measurements with Theory

The two independent sets of measurements agree within standard errors. Each set of measurements can be represented by wavelength dependencies of $\lambda'^{(-5.3 \pm 0.3)}$ and $\lambda^{(-4.6 \pm 0.3)}$ when normalized to units of photons and $\lambda'^{(-5.5 \pm 0.4)}$ and $\lambda^{(-4.8 \pm 0.3)}$ when normalized to units of energy. The relationship $\lambda^{(-4.8 \pm 0.3)}$ normalized to units of energy agrees with the previously measured wavelength dependence of λ^{-5} within standard error.¹³ These relationships are compared with one other set of measurements and several theoretical relationships that have been used in the past (Fig. 4). Shown are the results from our measurements, measurements by Sugihara *et al.*¹³ and Faris and Copeland,²⁷ the theoretical wavelength dependence³⁰ of λ^{-4} , a wavelength dependence of

Table 1. Exponents in the Wavelength Dependence of Raman Scattering by Pure Water

Normalization	Instrument	Incident Wavelength	Scattered Wavelength
Photons	PTI	-5.20 ± 0.05 (0.996)	-4.68 ± 0.04 (0.996)
	Hitachi	-5.3 ± 0.3 (0.92)	-4.6 ± 0.3 (0.92)
Energy	PTI	-5.33 ± 0.05 (0.996)	-4.80 ± 0.04 (0.996)
	Hitachi	-5.5 ± 0.4 (0.90)	-4.8 ± 0.3 (0.90)

The values in parentheses are the correlation coefficients of the fits (r^2). The errors represent standard errors in the exponent.

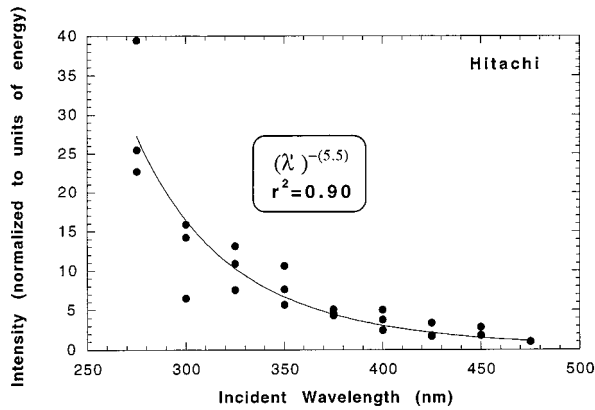


Fig. 3. Peak areas of Raman scattering, normalized to energy units, as a function of the incident wavelength (solid circles). These measurements were made with a Hitachi spectrofluorometer. The data are normalized at 475 nm. The solid curve shows the best fit of $(\lambda')^{-5.5}$ ($r^2 = 0.90$).

$(\lambda')^{-4}$ that has been used in the past,^{6,7} and relationships applicable to resonance Raman scattering,^{27,32,33} which is a function of both incident and scattered wavelengths.

Resonance Raman scattering occurs when the wavelength of the incident light approaches a wavelength of electronic or vibronic absorption of the substance. At wavelengths far from the absorption band, Raman scattering is expected to follow a λ^{-4} dependence. Closer to the absorption band, Raman scattering is expected to follow a wavelength dependence of approximately^{27,32,33}

$$b_{rw}(\lambda) \propto \frac{\nu^4}{[(\nu'')^2 - (\nu')^2]^2}, \quad (4)$$

where ν' and ν are the frequencies of the incident and scattered photons, respectively, and ν'' is the frequency of the intermediate energy level reached by the incident photon. In this study, the relevant intermediate energy level for water occurs at a wavelength of 130 nm.³⁴ At wavelengths even closer to the absorption band, Raman scattering is expected to follow a wavelength dependence of the form³³

$$b_{rw}(\lambda) \propto \nu^4 \frac{[(\nu'')^2 + (\nu')^2]^2}{[(\nu'')^2 - (\nu')^2]^4}. \quad (5)$$

The relationships compared here were normalized to one for an incident wavelength of 488 nm (corresponding to a scattered wavelength of 584 nm) [Fig. 4(a)]. This is the incident wavelength at which most previous measurements of the magnitude of the Raman-scattering coefficient of pure water have been made.^{5,13,21–24} This figure illustrates the increasing deviation with decreasing wavelength between estimated Raman-scattering coefficients when different wavelength dependencies are used. The wavelength dependence presented here shows close agreement with the experimental results of Sugihara *et al.*¹³ and Faris and Copeland²⁷ and the theoretical

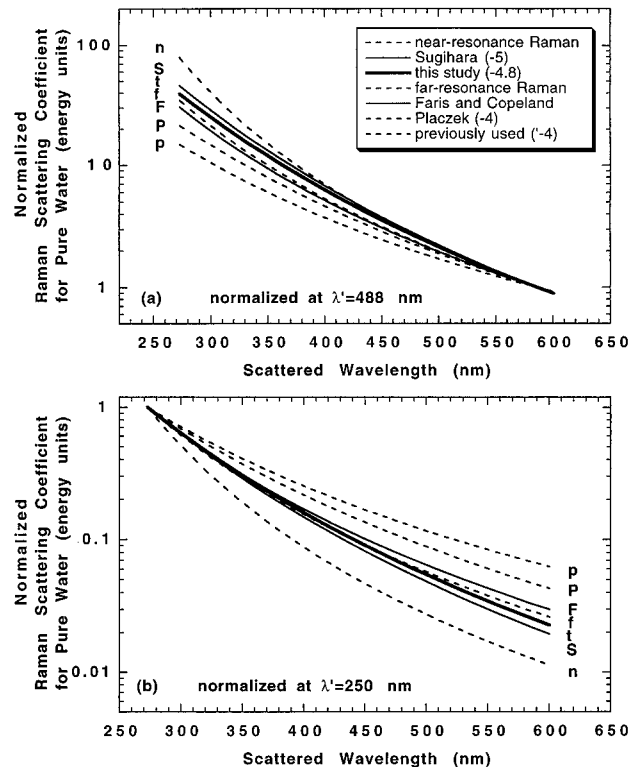


Fig. 4. Comparison of the wavelength dependence of Raman scattering by pure water normalized to energy units as a function of the scattered wavelength from various sources. Each of the curves shown were normalized at an incident wavelength of (a) 488 nm (or a scattered wavelength of 584 nm) and (b) 250 nm (or a scattered wavelength of 273 nm). The thick solid curve shows the results presented in this paper (curve t). The thin solid curves show the results from previously published measurements by Sugihara *et al.*¹³ (curve S) and Faris and Copeland²⁷ (curve F). The dashed curves show the theoretical relationships of λ^{-4} from Placzek³⁰ (curve P), two resonance Raman relationships (for wavelengths far from the absorption band [Eq. (4), curve f] and near the absorption band [Eq. (5), curve n], and the relationship of $(\lambda')^{-4}$ that has been used in previous studies (curve p).

relationship of relation (4) by use of an absorption wavelength of 130 nm.³⁴ However, it differs from the theoretical relationships of λ^{-4} and relation (5) and the previously used relationship of $(\lambda')^{-4}$ by as much as a factor of 4 near 300 nm when normalized at an incident wavelength of 488 nm. This indicates that Raman scattering by water is a resonance Raman-scattering process in the wavelength region studied here, following a wavelength dependence represented by relation (4). The differences observed between the different wavelength dependencies that have been used are further complicated by numerous conflicting reports regarding the absolute magnitude of the Raman-scattering coefficient for pure water for incident wavelengths of 488 nm.

3. Raman-Scattering Coefficient for Pure Water at 488 nm

The magnitude of $b_{rw}(488)$ for the 3400- cm^{-1} Raman line was determined with the PTI instrument. We

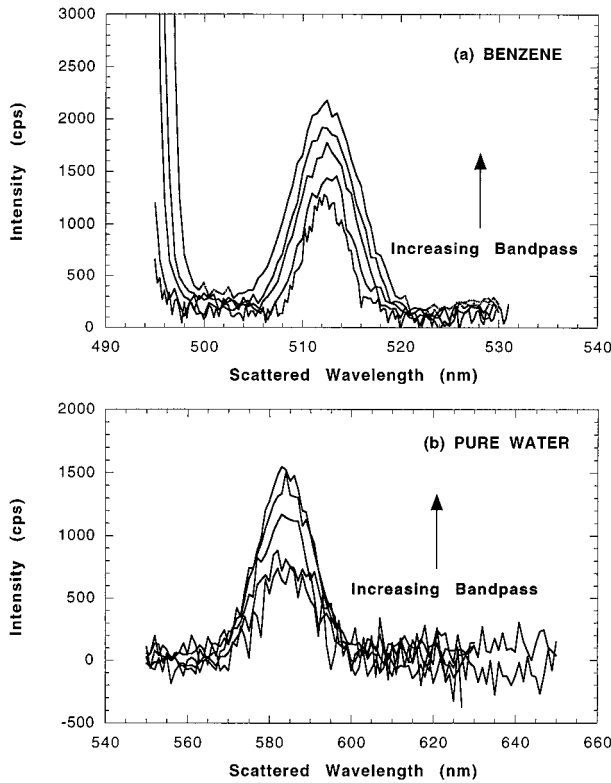


Fig. 5. Spectra resulting from Raman scattering for an incident wavelength of 488 nm with bandpasses ranging in value from 3.5 to 6 nm for (a) benzene and (b) pure water.

obtained the absolute magnitude by comparing Raman scattering by pure water with Raman scattering by spectroscopic-grade benzene, which has a scattering cross section of $(3.25 \pm 0.10) \times 10^{-29} \text{ cm}^2 \text{ sr}^{-1} \text{ molecule}^{-1}$ for the 992-cm^{-1} line when the incident wavelength is 488 nm.³⁵ Raman spectra were measured for steps of 1 nm, with an integration time of 5 s/step, over a range of bandpasses (3.5 to 6 nm) [Figs. 5(a) and 5(b)]. A bandpass of 2 nm (which was used by Marshall¹⁶) produced signal intensities that were too low to resolve the Raman peaks. Each of these spectra shows a distinct peak caused by Raman scattering that increases in magnitude with increasing bandpass [see Figs. 5(a) and 5(b)]. The strong peak evident to the left of the Raman peak in Fig. 5(a) is the Rayleigh peak at 488 nm. The Raman peaks were integrated to obtain the peak areas. The ratio of the peak areas for pure water and benzene, at corresponding bandpasses, could then be used to estimate $b_{rw}(488)$.^{5,13}

The peak areas for pure water and benzene are shown as a function of the bandpass in Fig. 6. According to theory,³⁶ the peak area (Φ) should increase as the square of the bandpass (β). Fitting quadratic equations to the peak areas for pure water and benzene, using a least-squares analysis, we obtained the relationships $\Phi_w = (707 \pm 22)\beta^2$ for pure water ($r^2 = 0.95$) and $\Phi_b = (512 \pm 13)\beta^2$ for benzene ($r^2 = 0.97$), where Φ_w is the peak area for Raman scattering by pure water and Φ_b is the peak area for Raman scattering

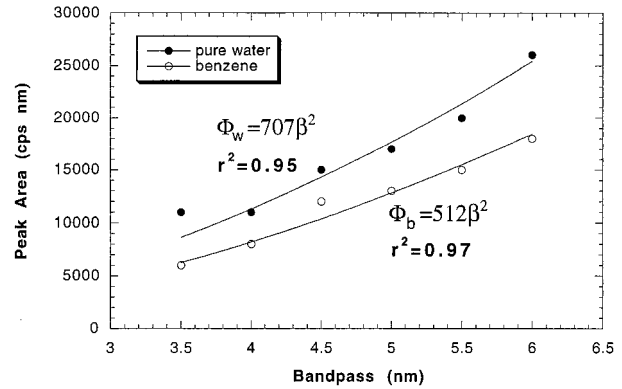


Fig. 6. Relationship between the peak areas of the Raman peaks and the bandpass for pure water (filled circles) and benzene (open circles). The data for each substance were fit by quadratics yielding $\Phi_w = 707\beta^2$ for pure water (with an r^2 determination coefficient of 0.95) and $\Phi_b = 512\beta^2$ for benzene ($r^2 = 0.97$).

by benzene (Fig. 6). The errors reported are standard errors in the coefficient. These relationships could be used to estimate $b_{rw}(488)$.

First, the scattering cross section of pure water at 90° [$(d\sigma_w/d\Omega)_{90^\circ}$] was calculated with the following relationship⁵:

$$\left(\frac{d\sigma_w}{d\Omega}\right)_{90^\circ} = \left(\frac{\Phi_w}{\Phi_b}\right) \left(\frac{n_w}{n_b}\right)^2 \left(\frac{T_b}{T_w}\right) \left(\frac{d_b}{d_w}\right) \left(\frac{M_w}{M_b}\right) \left(\frac{1 + \rho_w}{1 + \rho_b}\right) \left(\frac{d\sigma_b}{d\Omega}\right)_{90^\circ}, \quad (6)$$

where the subscripts b and w refer to benzene and pure water, respectively; σ is the scattering cross section; Ω is the solid angle; Φ is the integrated flux (or Raman peak area) at 90° ; n is the refractive index; T is the transmission of the liquid-quartz interface; d is the density; M is the molecular weight; and ρ is the depolarization ratio. Because (Φ_w/Φ_b) is the ratio of the peak areas for pure water and benzene, which in turn can be approximated by a ratio of two quadratic formulas, a simple manipulation yields $(\Phi_w/\Phi_b) = (707 \pm 22)/(512 \pm 13) = (1.38 \pm 0.08)$. The values for the remaining quantities used to evaluate Eq. (6) are listed in Table 2. They yield an estimate for $[d\sigma_w(488)/d\Omega]_{90^\circ}$ of $(8.4 \pm 0.5) \times 10^{-30} \text{ cm}^2 \text{ sr}^{-1} \text{ molecule}^{-1}$ (Table 2). Previously published estimates of $[d\sigma_w(488)/d\Omega]_{90^\circ}$ vary from 8.1×10^{-30} to $45 \times 10^{-30} \text{ cm}^2 \text{ sr}^{-1} \text{ molecule}^{-1}$, with most of the estimates at the lower end of the range.⁵ The result presented here agrees with several of the previously published values.^{5,22-27}

Next, from Kattawar and Xu,⁶ $b_{rw}(488)$ can be calculated from the scattering cross section, with the relationship

$$b_{rw}(\lambda) = \frac{800N\pi}{3} \left[\frac{d\sigma_w(\lambda)}{d\Omega} \right]_{90^\circ} \left(\frac{1 + 2\rho_w}{1 + \rho_w} \right), \quad (7)$$

where N is the number of molecules per cubic centimeter. This yields a value for $b_{rw}(488)$ of $(2.7 \pm 0.2) \times 10^{-4} \text{ m}^{-1}$ (Table 2). This result is not signifi-

Table 2. Values Used for the Calculation of the Raman-Scattering Coefficients $b_{rw}(488)$ for Pure Water and $b_{rs}(488)$ for Pure Seawater

Quantity	Benzene	Pure Water	Pure Seawater	Units
n	1.50 ^a	1.33 ^b	1.34 ^b	
T	1.00 ^c	0.98 ^c	0.98 ^c	
d	0.8787 ^a	0.998 ^b	1.025 ^b	g cm^{-3}
M	78.1	18.0	18.4 ^d	g mol^{-1}
ρ	0.02 ^c	0.17 ^c	0.17 ^c	
$(d\sigma(488)/d\Omega)_{90^\circ}$	$(32.5 \pm 1) \times 10^{-30e}$	$(8.4 \pm 0.5) \times 10^{-30}$	$(8.5 \pm 0.5) \times 10^{-30}$	$\text{cm}^2 \text{sr}^{-1} \text{molecule}^{-1}$
N	—	3.34×10^{22f}	3.35×10^{22f}	molecules cm^{-3}
$b_r(488)$	—	$(2.7 \pm 0.2) \times 10^{-4}$	$(2.7 \pm 0.2) \times 10^{-4}$	m^{-1}

^aRef. 37.

^bRef. 38.

^cRef. 5.

^dAssuming seawater consists of a 108:1 ratio of water molecules to Na^+ and Cl^- ions³⁹ (the main chemical constituents of seawater): $M = (108/109) \times 18.0 + (1/109) \times 58.4 = 18.4 \text{ g mol}^{-1}$.

^eRef. 35.

^f N (molecules cm^{-3}) = N_A ($\text{molecules mol}^{-1}$) d (g cm^{-3})/ M (g mol^{-1}), where $N_A = 6.022 \times 10^{23} \text{ molecules mol}^{-1}$.

cantly different from the value of $2.6 \times 10^{-4} \text{ m}^{-1}$ reported by Marshall and Smith.⁵

4. Raman Scattering by Seawater

To determine the magnitude of $b_{rs}(\lambda)$, measurements of Raman scattering by pure seawater at 90° were compared with similar measurements for pure water over a range of incident wavelengths (from 250 to 500 nm) with the PTI instrument. Two seawater samples [(1) aged, with a salinity of 36 practical salinity units (psu) and (2) ultrafiltered and UV oxidized, with a salinity of 31 psu] were used to represent pure seawater. The two sets of peak areas agree within experimental error (5%), indicating that the presence of the chloride ion and other chemical constituents in seawater have little effect on either the magnitude or the spectral variability of Raman scattering by pure water (Fig. 7). This result was stable for both samples of pure seawater available. Changing the values of the other quantities in Eqs. (6) and (7) to those

representative of seawater yielded only a 2% difference between computed $b_{rw}(488)$ and $b_{rs}(488)$ (Table 2). Recent examination of the influence of Raman scattering by seawater on Fraunhofer line depths in the ocean indicated that $b_{rs}(492)$ is approximately $2.6 \times 10^{-4} \text{ m}^{-1}$.^{25,26} Hence, it appears that $b_{rw}(\lambda)$ is an excellent approximation for $b_{rs}(\lambda)$.

5. Summary

Accurate estimates for the magnitude and spectral variability of $b_{rw}(\lambda')$ are necessary for modeling the effects of Raman scattering on reflectance and on the light transmission under water. Two sets of independent estimates for the spectral variability of the Raman-scattering coefficient of pure water for incident wavelengths in the 250–500-nm range have been presented, as well as an estimate for the magnitude of the Raman-scattering coefficient for pure water at 488 nm. Similar estimates for pure seawater are also presented. The main results from this study can be summarized as follows:

The coefficients $b_{rw}(\lambda')$ and $b_{rs}(\lambda)$ appear to follow spectral dependencies of $(\lambda')^{-5.3 \pm 0.3}$ and $\lambda^{-4.6 \pm 0.3}$, respectively, when normalized to units of photons. The corresponding relationships when normalized to units of energy are $(\lambda')^{-5.5 \pm 0.4}$ and $\lambda^{-4.8 \pm 0.3}$. The exponents of these spectral results agree with measurements made by Sugihara *et al.*¹³ within standard error and show close agreement with measurements of Faris and Copeland.²⁷ Other previously used exponents for the spectral shape of $b_{rw}(\lambda')$ differ from the results presented here by as much as 26%. The spectral dependence appears to follow a wavelength dependence consistent with resonance Raman theory, with an absorption wavelength of 130 nm. Care must be taken to use the relationship normalized to units appropriate to the study under investigation.

The absolute magnitude for $b_{rw}(488)$ was found to take a value of $(2.7 \pm 0.2) \times 10^{-4} \text{ m}^{-1}$. This value is in general agreement with the results of Marshall and Smith,⁵ Kondilenko *et al.*,²⁴ Chang and Young,²² Romanov and Shuklin,²³ and Faris and Copeland.²⁷

The Raman-scattering coefficients of seawater

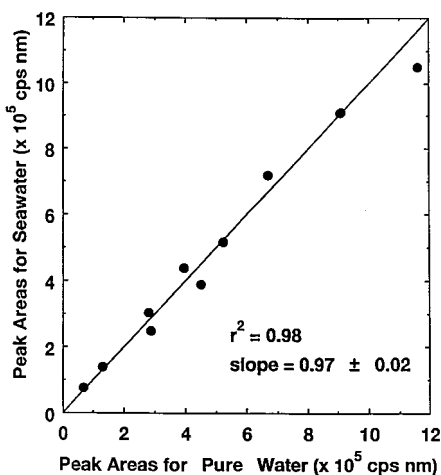


Fig. 7. Peak areas for Raman scattering by pure seawater plotted against peak areas for Raman scattering by pure water at the same wavelength (filled circles). The solid line is the 1:1 line. The r^2 determination coefficient for the peak areas is 0.98, with a slope of 0.97 ± 0.02 .

$[b_{rs}(\lambda)]$ and pure water $[b_{rw}(\lambda)]$ were found to agree within experimental uncertainty, both in their absolute magnitudes and in their spectral characteristics. It is suggested that $b_{rw}(\lambda)$ can be used as an adequate approximation for $b_{rs}(\lambda)$ to model Raman scattering by seawater in the UV and visible regions.

We thank T. Platt for his help and support; R. Zika for the use of his instrument; V. Lutz, E. Head, and B. Irwin for their help with part of the experimental research presented; and P. Kepkey and B. MacDonald for providing seawater and pure water samples. We also acknowledge the help we received from D. Fraser (PTI). We thank J. Coxon for many helpful discussions. The comments and suggestions offered by an anonymous reviewer in the earlier stages of this research were extremely helpful to improve our results. We also thank V. Haltrin for helpful comments on the manuscript. We gratefully acknowledge the support provided by the U.S. Office of Naval Research; the National Aeronautics and Space Administration; the Canadian Department of Fisheries and Oceans; and the Natural Sciences and Engineering Research Council of Canada. Part of this research was carried out as part of the Canadian contribution to the Joint Global Ocean Flux Study.

References

1. T. Platt and S. Sathyendranath, "Oceanic primary production: estimation by remote sensing at local and regional scales," *Science* **241**, 1613–1620 (1988).
2. S. Sathyendranath, T. Platt, E. P. W. Horne, W. G. Harrison, O. Ulloa, R. Outerbridge, and N. Hoepffner, "Estimation of new production in the ocean by compound remote sensing," *Nature (London)* **353**, 129–133 (1991).
3. M. R. Lewis, M.-E. Carr, G. C. Feldman, W. Esaias, and C. McClain, "Influence of penetrating solar radiation on the heat budget of the equatorial Pacific Ocean," *Nature (London)* **347**, 543–545 (1990).
4. R. H. Stavn and A. D. Weidemann, "Optical modeling of clear ocean light fields: Raman scattering effects," *Appl. Opt.* **27**, 4002–4011 (1988).
5. B. R. Marshall and R. C. Smith, "Raman scattering and in-water ocean optical properties," *Appl. Opt.* **29**, 71–84 (1990).
6. G. W. Kattawar and X. Xu, "Filling in of Fraunhofer lines in the ocean by Raman scattering," *Appl. Opt.* **31**, 6491–6500 (1992).
7. Z. Lee, K. L. Carder, S. K. Hawes, R. G. Steward, T. G. Peacock, and C. O. Davis, "An interpretation of high spectral resolution remote sensing reflectance," in *Optics of the Air-Sea Interface: Theory and Measurement*, L. Estep, ed., Proc. SPIE **1749**, 49–64 (1992).
8. Y. Ge, H. R. Gordon, and K. J. Voss, "Simulation of inelastic-scattering contributions to the irradiance field in the ocean: variation in Fraunhofer line depths," *Appl. Opt.* **32**, 4028–4036 (1993).
9. V. I. Haltrin and G. W. Kattawar, "Self-consistent solutions to the equation of transfer with elastic and inelastic scattering in oceanic optics. 1. Model," *Appl. Opt.* **32**, 5356–5367 (1993).
10. S. Sathyendranath and T. Platt, "Angular structure of under-water light field: importance for ocean-colour models," in *Ocean Optics XIII*, S. G. Ackleson and R. Frouin, eds., Proc. SPIE **2963**, 26–31 (1997).
11. C. D. Mobley, *Light and Water: Radiative Transfer in Natural Waters* (Academic, San Diego, Calif., 1994).
12. J. S. Bartlett, "A comparison of models of sea-surface reflectance incorporating Raman scattering by water," in *Ocean Optics XIII*, S. G. Ackleson and R. Frouin, eds., Proc. SPIE **2963**, 592–596 (1997).
13. S. Sugihara, M. Kishino, and N. Okami, "Contribution of Raman scattering to upward irradiance in the sea," *J. Oceanogr. Soc. Jpn.* **40**(6), 397–404 (1984).
14. R. H. Stavn and A. D. Weidemann, "Raman scattering effects in ocean optics," in *Ocean Optics IX*, M. A. Blizard, ed., Proc. SPIE **925**, 131–139 (1988).
15. R. H. Stavn and A. D. Weidemann, "Raman scattering in ocean optics: quantitative assessment of internal radiant emission," *Appl. Opt.* **31**, 1294–1303 (1992).
16. B. R. Marshall, "Raman scattering in ocean water," M.A. thesis (University of California at Santa Barbara, Santa Barbara, Calif., 1989).
17. R. H. Stavn, "Raman scattering effects at the shorter visible wavelengths in clear ocean waters," in *Ocean Optics X*, R. W. Spinrad, ed., Proc. SPIE **1302**, 94–100 (1990).
18. R. H. Stavn, "Effects of Raman scattering across the visible spectrum in clear ocean water: a Monte Carlo study," *Appl. Opt.* **32**, 6853–6863 (1993).
19. V. I. Haltrin, G. W. Kattawar, and A. D. Weidemann, "Modeling of elastic and inelastic scattering effects in oceanic optics," in *Ocean Optics XIII*, S. G. Ackleson and R. Frouin, eds., Proc. SPIE **2963**, 597–602 (1997).
20. J. S. Bartlett, "The influence of Raman scattering by seawater and fluorescence by phytoplankton on ocean colour," M.S. thesis (Dalhousie University, Halifax, Nova Scotia, 1996).
21. R. B. Slusher and V. E. Derr, "Temperature dependence and cross sections of some Stokes and anti-Stokes Raman lines in ice Ih," *Appl. Opt.* **14**, 2116–2120 (1975).
22. C. H. Chang and L. A. Young, "Seawater temperature measurement from Raman spectra," Research Note 920, N62269-72-C-0204 (Advanced Research Projects Agency, Washington, D.C., July 1972).
23. N. P. Romanov and V. S. Shuklin, "Raman scattering cross section of liquid water," *Opt. Spectrosc. (USSR)* **38**, 646–648 (1975).
24. I. I. Kondilenko, P. A. Korotkov, V. A. Klimenko, and O. P. Demyanenko, "Transverse cross section of the Raman scattering of the ν_1 vibration of the water molecule in the liquid and gaseous states," *Opt. Spectrosc. (USSR)* **43**, 384–386 (1977).
25. C. Hu and K. J. Voss, "Solar stimulated inelastic light scattering in clear sea water," in *Ocean Optics XIII*, S. G. Ackleson and R. Frouin, eds., Proc. SPIE **2963**, 266–271 (1997).
26. C. Hu and K. J. Voss, "In situ measurements of Raman scattering in clear ocean water," *Appl. Opt.* **36**, 6962–6967 (1997).
27. G. W. Faris and R. A. Copeland, "Wavelength dependence of the Raman cross section for liquid water," *Appl. Opt.* **36**, 2686–2688 (1997).
28. J. W. Hofstraat and M. J. Latuhipin, "Correction of fluorescence spectra," *Appl. Spectrosc.* **48**, 436–447 (1994).
29. Y. Ge, "Measurement of inelastic scattering in the ocean," M.S. thesis (University of Miami, Coral Gables, Florida, 1993).
30. G. Placzek, ed., *Marx Handbuch der Radiologie*, 2nd ed. (Academische Verlagsgesellschaft, Leipzig, 1934), Vol. 6.
31. G. W. Chantry, "Polarizability theory of the Raman effect," in *The Raman Effect: Principles*, A. Anderson, ed. (Marcel Dekker, New York, 1971), Vol. 1.
32. W. K. Bischel and G. Black, "Wavelength dependence of Raman scattering cross sections from 200–600 nm," in *Excimer Lasers—1983*, C. K. Rhodes, H. Egger, and H. Pummer, eds. (American Institute of Physics, New York, 1983), 181–187.
33. J. Tang and A. C. Albrecht, "Developments in the theories of vibrational Raman intensities," in *Raman Spectroscopy*, H. A. Szymanski, ed. (Plenum, New York, 1970), 33–68.
34. L. R. Painter, R. D. Birkhoff, and E. T. Arakawa, "Optical

- measurements of liquid water in the vacuum ultraviolet," *J. Chem. Phys.* **51**, 243–251 (1969).
35. Y. Kato and H. Takuma, "Absolute measurement of Raman-scattering cross sections of liquids," *J. Opt. Soc. Am.* **61**, 347–350 (1971).
36. R. Kingslake, ed., *Applied Optics and Optical Engineering* (Academic, New York, 1965), Vol. 1.
37. J. G. Grasselli and W. M. Ritchey, *Atlas of Spectral Data and Physical Constants for Organic Compounds*, 2nd ed. (CRC Press, Cleveland, Ohio, 1975), Vol. 2.
38. D. E. Gray, ed., *American Institute of Physics Handbook*, 3rd ed. (McGraw-Hill, New York, 1972).
39. D. R. Lide, ed., *Handbook of Chemistry and Physics*, 72nd ed. (CRC Press, Boston, Mass., 1991).